Science of the Total Environment 724 (2020) 138309

Contents lists available at ScienceDirect

Science of the Total Environment

journal homepage: www.elsevier.com/locate/scitotenv

On-line determination of soluble Zn content and size of the residual fraction in $PM_{2.5}$ incubated in various aqueous media

Zhiqiang Tan [a,*], Qingsheng Bai [a,b], Yongguang Yin [a], Yang Zhang [b], Qiang Chen [a,c], Myeong Hee Moon [d], Jingfu Liu [a,b]

[a] State Key Laboratory of Environmental Chemistry and Ecotoxicology, Research Center for Eco-Environmental Sciences, Chinese Academy of Sciences, Beijing 100085, China
[b] College of Resources and Environment, University of Chinese Academy of Sciences, Beijing 100049, China
[c] College of Environment and Ecology, Chengdu University of Technology, Chengdu 610059, China
[d] Department of Chemistry, Yonsei University, Seoul 03722, South Korea

HIGHLIGHTS

- Soluble Zn in $PM_{2.5}$ is strongly associated with its bioaccessibility.
- Quantification and size characterization were achieved in one run.
- The soluble Zn fractions in $PM_{2.5}$ incubated in simulated lung fluid were over 40%.
- The amount of particles released in simulated lung fluid was significantly high.

GRAPHICAL ABSTRACT

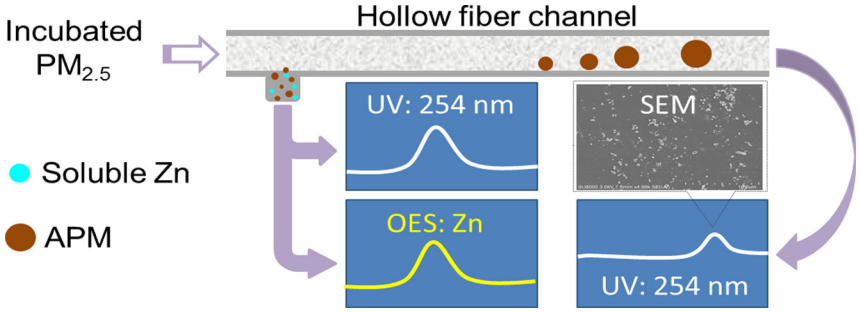

ARTICLE INFO

Article history:
Received 5 February 2020
Received in revised form 27 March 2020
Accepted 28 March 2020
Available online 30 March 2020

Editor: Jianmin Chen

Keywords:
Soluble zinc
Size characterization
$PM_{2.5}$
Hollow fiber flow field-flow fractionation
Simulated lung fluid

ABSTRACT

Transition metals in airborne particulate matter, especially those with aerodynamic diameters no more than 2.5 μm ($PM_{2.5}$), have attracted considerable attention due to their potential environmental and human health risks. However, determination of these potential risks requires comprehensive knowledge of their dissolution behavior and residual size in aqueous media. Herein, we describe an analytical method for on-line determination of the soluble fraction of Zn as a model transition metal and the size of residual $PM_{2.5}$ using hollow fiber flow field-flow fractionation (HF5) coupled with UV–vis absorption spectroscopy and inductively coupled plasma optical emission spectroscopy. HF5 was directly applied on the incubated samples in pure water (PW), simulated natural water (SNW), and simulated lung fluid (SLF) due to its efficient in-line filtration and excellent fractionation resolution. Firstly, the potential of the proposed method (under optimized conditions) for size characterization was assessed against commercial silica microparticles, and results in good agreement with manufacturer and scanning electron microscopy values were obtained. The accuracy of quantification of soluble Zn in various media was then validated using a standard reference material in terms of satisfactory recoveries compared with the reference values. For the real $PM_{2.5}$ samples collected from different sites in Beijing, China, the soluble Zn percentages in PW, SNW, and SLF were within 15.4–16.7%, 10.6–12.7%, and 43.1–46.9%, respectively, with the amount of particles smaller than ~10 nm released from $PM_{2.5}$ increasing in the order of SNW < PW < SLF. The proposed HF5-based method provides a powerful and efficient tool for the quantification of soluble transition metal fractions and size characterization of residual particles with reduced analysis times, thus possessing great promise in real-time tracking of the transformation of $PM_{2.5}$ in environmental and physiological media and in risk assessment.

* Corresponding author.
E-mail address: zqtan@rcees.ac.cn (Z. Tan).

https://doi.org/10.1016/j.scitotenv.2020.138309
0048-9697/

1. Introduction

Due to the rapid growth of industrialization and urbanization in recent years, the release of airborne particulate matter (APM) has increased considerably (Akimoto, 2003; Gupta et al., 2006; Zhang et al., 2019). APM related issues has drawn a growing attention globally, especially in China and other developing countries, mainly due to its adverse effects on air quality, climate, ecosystems, and human health (Castro-Jimenez et al., 2017; Fuzzi et al., 2015; Amini et al., 2019; Kim et al., 2015). Fine APM, with aerodynamic diameters no more than 2.5 μm ($PM_{2.5}$), is widely regarded as the dominant contributor to human health risk (Bell et al., 2007; Song et al., 2017). A series of epidemiological studies have demonstrated a strong association between adverse health effects (e.g., respiratory, cardiovascular, and pulmonary diseases) and exposure to $PM_{2.5}$ (Pun et al., 2017; Gu et al., 2017). Therefore, determination of the $PM_{2.5}$ concentration is crucial to evaluate the air quality as suggested by the World Health Organization (WHO) (WHO, 2006). Nevertheless, this range of APM has not been comprehensively characterized to fully understand its adverse effects.

Chemical and morphological (e.g., size) characteristics are the fundamental parameters of $PM_{2.5}$ governing their health risks. Given the multiple sources, both natural and anthropogenic, contributing to the composition of $PM_{2.5}$, this mixture of inorganic and organic compounds is extremely complex and considerably varies between regions (Bell et al., 2007; Bressi et al., 2013). With regards to the inorganic components, in vitro and in vivo toxicological studies have demonstrated the exposure–risk relationship of transition metals on various living organisms (Rice et al., 2001; Hu et al., 2012). For example, excessive ingestion of Zn, an essential element required for human health, may also lead to a number of serious health problems such as anemia (Porea et al., 2000), hypertension (Suarez-Varela et al., 2015), and Alzheimer's disease (Rychlik and Mlyniec, 2020). Specifically, it has been found that Zn-induced injury to lung may be due to the generation of toxic reactive oxygen species such as superoxide anion radicals (Maret and Sandstead, 2006). Moreover, further studies concluded that soluble fractions of transition metals correlated more strongly with the amount of reactive oxygen species than the particulate fraction (Song et al., 2010). This indicates that the quantification of soluble transition metals instead of their total content will provide a more accurate estimation of bioaccessible transition metals in $PM_{2.5}$. Furthermore, it has been experimentally shown that ultrafine sized particles (e.g., in nanometer size) can more easily enter organs and tissues as well as the circulatory system, subsequently posing much greater toxicity than micrometer-sized particles (Stone et al., 2007; Allen et al., 2014; Calderon-Garciduenas et al., 2008). Therefore, a greater understanding on the size of the soluble transition metal residual fraction of $PM_{2.5}$ will lead to improved risk assessment of $PM_{2.5}$-related adverse health effects.

Considerable research has been conducted to determine the soluble fractions of transition metals in $PM_{2.5}$ by extraction, using a sequential leaching procedure. Generally, pure water (PW) is used as the leaching agent in the estimation of bioaccessibility and toxicity (Chan et al., 2016; Mukhtar and Limbeck, 2010). This medium is suitable to estimate the dissolution behavior of transition metals in $PM_{2.5}$ in a natural aqueous environment. Recently, other leaching agents, such as simulated human body fluids, have been employed to obtain a more realistic understanding of the soluble fraction of transition metals in physiological environments (Zereini et al., 2012; Gao et al., 2018). In order to reduce or eliminate matrix background interference, pretreatment of samples, such as centrifugation and filtration, is frequently needed to remove insoluble fractions. Subsequently, off-line characterization methods, such as scanning electron microscopy (SEM), are required to assess the size of the collected residual fractions. SEM provides accurate particle size determinations of the residual fractions, yet it requires tedious and time-consuming procedures, including sample preparation and calculation of results as well as strict operations (Loxham et al., 2013). To overcome these drawbacks, it would be preferable to develop dual functional analytical methods for the simultaneous quantification of soluble fractions and size characterization.

Field-flow fractionation (FFF) has evolved as one of the most powerful tools for the size characterization of macromolecules and particles. Sub-techniques of FFF are defined by the external force imposed, e.g., flow field gives rise to the subclass of flow FFF (Giddings, 1993). Among the different variants of flow FFF, hollow fiber flow FFF (HF5) employs a disposable hollow fiber (HF) as the separation channel instead of the conventional rectangular channel, leading to a technique with low cost, flexible operation, and miniaturization (Lee et al., 1999; van Bruijnsvoort et al., 2001; Zattoni et al., 2007). Of note, the separation size range by HF5 is theoretically from 1 nm to 100 μm, indicating that it is widely applicable for the separation of nanoparticles as well as microparticles (Zattoni et al., 2007). The powerful separation ability of HF5 has been used for the characterization and determination of seven Ag species, including various Ag(I) species (i.e., free Ag(I), weak and strong Ag(I) complexes) and different-sized Ag nanoparticles (AgNPs), with the retention time of AgNPs increasing with their increase in hydrodynamic size (Tan et al., 2015). Furthermore, the excellent in-line filtration function of HF5 was shown to track transformations of trace AgNPs and Ag(I) under environmentally relevant concentrations (Tan et al., 2017). Interestingly, for microparticles, where the hydrodynamic lift force becomes dominant in fractionation, the elution order was opposite to that observed for nanoparticle, i.e., the large particles elute earlier than the small ones, following the principle termed as the steric/hyperlayer mode of HF5 (Min et al., 2002). Since its discovery, HF5 operated in the steric/hyperlayer mode paved a way for size characterization of different micrometer-sized particles such as biological macromolecules, bacteria, and cells (Reschiglian et al., 2002, 2003; Zattoni et al., 2008), but it has rarely been used for environmental microparticle analysis. HF5 coupled with UV–vis absorption spectroscopy (UV) was used to assess the size and size distribution of airborne particle fractions obtained by split-flow thin fractionation over a decade ago (Kim et al., 2006), clearly demonstrating the high speed and accuracy of HF5 in the size characterization of APM compared with SEM. Therefore, this technique was herein employed to characterize the size of the residual fractions of $PM_{2.5}$. Further, the potential applicability of HF5 to simultaneously determine the soluble transition metal content and the size of the residual fraction was explored.

We herein present a dual functional approach for the quantification of the soluble fractions of Zn as the model transition metal in $PM_{2.5}$ and size characterization of the residual fraction in one run. The instrumentation mainly consisted of HF5 to separate the soluble and residual fractions, UV detector for size characterization of the residual fractions, and inductively coupled plasma optical emission spectrometry (ICPOES) for the identification and quantification of soluble Zn. The key parameters affecting the separation of HF5 were optimized using standard polystyrene microparticles (PS MPs). The method's accuracy for size characterization was tested by comparing the results for commercial silica microparticles (SiO_2 MPs) with those obtained by SEM as well as the nominal values. Furthermore, the reliability of the approach for quantifying soluble Zn fractions in three different aqueous media, including PW, simulated natural water (SNW), and simulated lung fluid (SLF), was evaluated using a standard reference material (SRM) according to the recovery results. Finally, the developed approach was applied for the quantification of soluble Zn in the three aqueous media as well as the size characterization of the corresponding residual fractions in $PM_{2.5}$ samples, collected at three sites in Beijing, China.

2. Materials and methods

2.1. Chemicals and materials

Five different sized National Institute of Standards and Technology (NIST) traceable size standards of PS MPs (1, 2, 3, 4, and 5 μm) were purchased from Thermo Fisher Scientific, Inc. (Waltham, Massachusetts,

USA), and employed to establish calibration plots for size characterization. A commercial stock colloid of SiO_2 MPs (nominal size, 2.47 μm) was obtained from Polysciences, Inc. (Warrington, Pennsylvania, USA). Standard solution of Zn (100 μg/mL) was bought from National Nonferrous Metals and Electronic Materials Analysis and Testing Center (Beijing, China). The analysis of soluble Zn fractions was validated using the SRM of urban particulate matter (1648a) obtained from NIST (Gaithersburg, USA). Sodium dodecyl sulfonate (SDS), acquired from ANPEL Laboratory Technologies (Shanghai, China) was used to prepare the carrier solution with Milli-Q water (Millipore, Bedford, MA, USA). A natural organic matter (NOM) stock solution (0.1 mg/mL C) was prepared by dissolving the Suwannee River NOM powder (1R101N) obtained from the International Humic Substances Society (Minnesota, USA) in ultrapure water (Shen et al., 2015). Polyacrylonitrile (PAN) HF (Synopex, Pohang, South Korea) with a molecular weight cut-off of 30 kDa enveloped in a silica tubes was used as the separation channel.

The SNW was prepared by spiking 10 mg/L C NOM in ultrapure water, followed by adjustment of pH to 5.0. An artificial lysosomal fluid (ALF), serving as the SLF, was used to evaluate the solubility of APM in the physiological environment within the lung. ALF was prepared according to previous studies (Zereini et al., 2012; Colombo et al., 2008), and its composition is given in the Supporting Information (SI) (Table S1). All chemicals in Table S1 were analytical grade reagents and used without further purification. The final pH of the SLF was also adjusted to pH 5.0 prior to use.

2.2. Apparatus and instruments

Fig. 1 depicts the homemade HF5 systems successively coupled with a UV detector and ICPOES (HF5-UV-ICPOES), which was modified from our previous studies (Lee et al., 1999; Tan et al., 2015). Briefly, as the key part for separation, the PAN HF inserted into a silica tube were 21 cm in length, 0.80 mm for the inner diameter, and 1.55 mm for the outer diameter. Specifically, to alleviate band broadening of the elute peak, the HF module was placed in an upright direction (Kim et al., 2006). For detection, UV detector provides the retention time of the eluted particles, which were further used for size calibration, and ICPOES was used to quantify soluble Zn content. The main operation parameters of UV detector and ICPOES are provided in Table S2.

The carrier solution was delivered by a plunger pump (1200, Agilent, USA) equipped with a degasser. The sample was injected into the flow path with a model 7752i injection valve (Rheodyne, Cotati, California, USA) with a 20-μL loop. The typical HF5 separation procedure involved two steps – focusing/relaxation and elution – which were triggered and converted by three electronically controlled valves (VICI, Valco Co., Houston, Texas, USA), namely a four-way one (V1) and two three-way valves (V2 and V3) in Fig. 1. Following sample injection, the focusing/relaxation step was performed by simultaneously delivering the carrier solution into the inlet and outlet of the HF (dotted line connection at V1 and V2). A metering valve (MV1) was used to adjust the ration of these two flow rates of the carrier solution to guarantee a focusing/relaxation point near the 10% of the entire fiber length. During this step, the soluble fraction was gradually filtrated out of the HF channel through the pores on the HF surface, and delivered by the radial flow out of the silica tubes and to the detection system via V3. After a proper time (e.g., 8 min), known as the focusing time, the elution step was carried out by respectively switching V1 directly to HF, V2 to the detector direction, and V3 to the waste (solid line connection at V1 and V2). During this step, the residual particles eluted according to their size, and were detected by UV detector and ICPOES in sequence. Additionally, an identical radial flow rate dominating the flow field was maintained during the whole run, which was achieved by another metering valve (MV2).

SEM images were obtained with a Hitachi Model JEM-2100F instrument (Hitachi Scientific Instruments, Nissei Sangyo America, Inc., Mountain View, California, USA), which were used to examine the size of the microparticles (i.e., SiO_2 MPs and the residual APM).

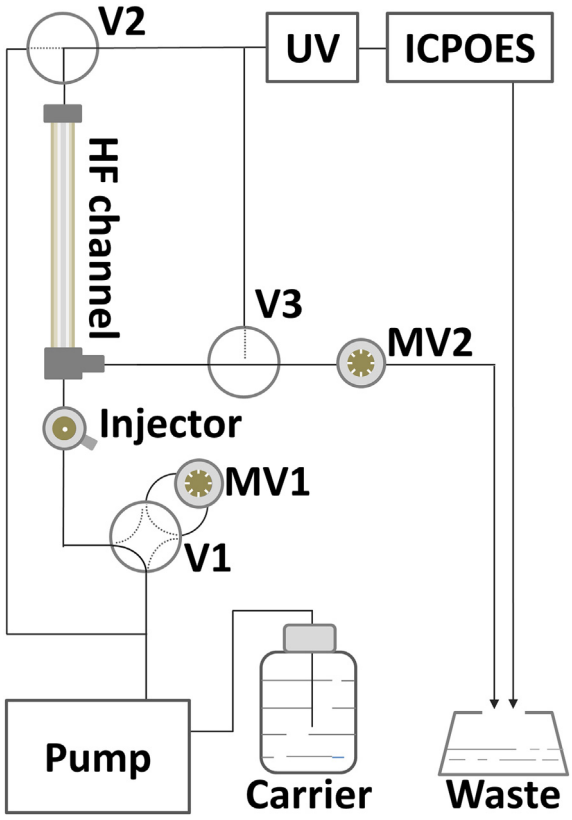

Fig. 1. Schematic diagram of the HF5-UV-ICPOES system. V1, four-way electronically controlled valve; V2, V3, three-way electronically controlled valves; MV1, MV2, metering valves.

2.3. Airborne particle sampling

Samples were collected during a sampling campaign conducted between October 30th, 2017 and November 6th, 2017 at three sampling sites – one on the roof of an inpatient building (~25 m above ground) located within the Second Ring Road of Beijing (R2) (39° 92′ N, 116° 40′ E), another on the roof of a teaching building (~30 m above ground) located near the Fourth Ring Road of Beijing (R4) (39° 91′ N, 116° 24′ E), and a last one on the roof of another teaching building (~20 m above ground) located outside the Sixth Ring Road of Beijing (R6) (40° 40′ N, 116° 69′ E). A map of the three sampling sites is shown in Fig. S1. $PM_{2.5}$ sampling was collected on quartz filters by an automated sampling system developed by the Zhang group (Huang et al., 2016). Following moisture equilibration at room temperature for 24 h, the filters were weighted before and after sampling to calculate the mass of $PM_{2.5}$ collected, which were performed at least three times in light of the weight uncertainty. The filters were subsequently stored in Petri dishes until analysis. Handling of the filters throughout sampling and analysis was performed using ceramic forceps and scissors to prevent metal contamination.

2.4. Dissolution behavior of Zn in PW, SNW, and SLF and analysis

To validate the accuracy and recovery of the HF5-UV-ICPOES system, about 10 mg of NIST SRM 1648a were accurately weighted and further incubated in each of the tested aqueous solutions. The mixtures were kept in a shaking incubator (IKA ® KS4000 i control, Germany) and maintained at 37 °C in the dark. After 12 h, 20 μL of the suspension was immediately injected into the HF5-UV-ICPOES system for

quantification of the soluble Zn fraction. For comparison, the remaining suspension was centrifuged at 12000 *g* for 20 min, and the contents of Zn in the supernatant and the sediments were determined by ICPOES after digestion by a microwave digestion system (CEM Corporation MARS-5, Matthews, North Carolina, USA). The digestion was performed using 1:5 v/v mixture of hydrofluoric acid and concentrated nitric acid in Teflon vessels with programmed temperature and time settings (heated to 100 °C at 20 °C/min and held for 1 min, heated to 150 °C at 10 °C/min and held for 1 min, heated to 185 °C at 7 °C/min and held for 35 min, and finally cooled to room temperature within 45 min). Based on the difference between the determined values in the sediment and the certified values, Zn content in the supernatant was calculated and used to evaluate accuracy of the proposed HF5-UV-ICPOES method.

The dissolution behavior assessment of Zn in real $PM_{2.5}$ samples was conducted by immersing the small pieces of quartz filter cut from a quarter of the filter into a plastic centrifuge tube containing 0.5 mL of the tested medium (pH 5.0). The mixtures were treated in the same way as NIST SRM 1648a above. After 12 h, 20 μL of the suspension was immediately injected into the HF5-UV-ICPOES system for quantification of the soluble Zn fraction and size characterization of the residual fraction. The remaining suspension was centrifuged, and the supernatant and the sediments as well as the remaining quarter of the sample and blank filters were subjected to microwave digestion under the same conditions described above. The digested solutions were used to validate the results obtained from the HF5-UV-ICPOES systems. To validate the size information generated by the HF5-UV-ICPOES system, the size of the residual fraction collected at the bottom of the centrifuge tubes was characterized by SEM. All samples were analyzed in triplicate, and the same sized blank filter as the sample filter were treated and analyzed simultaneously.

3. Results and discussion

3.1. Optimization and performance of the HF5 system

In order to evaluate the separation and characterization of micrometer-sized particles by the HF5 system, parameters including carrier liquid, radial flow rate, focusing time, and axial flow rate were optimized using PS MPs based on their separation resolution (*Rs*), which was equal to twice the difference of the retention time divided by the sum of the width of the sample peak positions (Tan et al., 2015). Specifically, the retention time was calculated by subtracting the focusing/relaxation time and the time required for the sample to travel through the outside of the separation channel from the elution time.

The carrier liquid composition, focusing time and flow rates, including radial and axial direction rates, are the fundamental parameters in the performance evaluation of the HF5 for size characterization (Zattoni et al., 2007). It has been demonstrated that a surfactant serving as the dispersing agent could significantly reduce unexpected particle–particle and particle–wall interactions (Carlshaf and Jönsson, 1991; Kim et al., 2012), proving its importance for improved separation and sample recovery. Among the various surfactants widely used in flow FFF, SDS and FL-70 have been demonstrated to be the most effective additives to enhance the separation of regular spherical particles as well as other non-spherical objects (e.g., carbon nanotubes) (Stevenson and Preston, 1997; Dubascoux et al., 2008). However, the latter surfactant contains ethylenediaminetetraacetic acid disodium, which may chelate with most transition metals and thus affect their dissolution behavior. Herein, separation of 1, 2, 3, 4, and 5 μm PS MPs was achieved with a carrier liquid containing 0.05% (m/V) SDS (Fig. S2A). A further increase in SDS concentrations beyond 0.05% (m/V) contributed little to improving separation resolution, but readily tended to form foam and bubbles in the carrier solution. Moreover, effects of setting parameters of the HF5 system such as focusing time, radial flow rate, and axial flow rate on the separation resolution of 4 and 5 μm PS MPs were systematically studied in the ranges of 2–8 min (Fig. S2B), 0.1–0.6 mL/min (Fig. S2C), and 1.5–3.0 mL/min (Fig. S2D), respectively. The optimized conditions were as follows: the carrier liquid, 0.05% (m/V) SDS, was delivered at the flow rate of 0.25 mL/min during the focusing/relaxation step; After focusing for 8 min, the rate was increased to 2.5 mL/min, where the metering valve (MV2 in Fig. 1) was employed to make that the radial flow rate and the axial flow rate were 0.25 and 2.25 mL/min, respectively.

The reproducibility of the HF5-based system was estimated by injecting five replicates of mixed standard solution of 4 and 5 μm PS MPs under the optimized conditions. The mean retention times of 4 and 5 μm PS MPs were 1.85 min with 0.5% relative standard deviation (RSD) ($n = 5$) and 1.36 min with 0.6% RSD ($n = 5$), respectively, along with a mean *Rs* value of 5.95 with 1.8% RSD ($n = 5$), indicating an excellent reproducibility of the system in the steric/hyperlayer mode.

For HF5 in the steric/hyperlayer mode, a series of standard particles of known particle size are commonly used to calibrate the size and size distribution of sample particles based on an empirical relationship between retention time (t_R) and particle diameter (d), given as the following equation: $\log t_R = \log t_{R1} - S \times \log d$, where t_{R1} is the extrapolated retention time per unit diameter and S is the diameter-based selectivity, defined as the absolute value of the slope of the fitted straight line (Reschiglian et al., 2003). The resolving capability of the HF5-based method for the size range of 1–5 μm PS MPs was plotted (Fig. 2A). There was a linear relationship between $\log t_R$ and $\log d$, with a squared correlation coefficient of 0.994 and t_{R1} of ~6.24 and S of ~0.90 (Fig. 2B), indicating that the HF5 herein has a comparable fractionating performance to the previously reported techniques (Reschiglian et al., 2003). Thus, on the basis of the calibration function, the retention time of microparticles of unknown size enables their size characterization.

3.2. Validation of HF5 system for size characterization with commercial SiO_2 MPs

Silica is the major inorganic component of particulate environmental samples (e.g., APM) (Yang et al., 2019), making it highly appropriate to test the performance of the proposed method for size characterization of the residual fraction of APM. Fedotov et al. recently optimized the parameters of a novel FFF instrument in a rotating coiled column using submicron-sized silica beads (Fedotov et al., 2014), and further extended this instrument for the fractionation of street dust (Fedotov et al., 2015). The peak of SiO_2 MPs appeared at the elution time of 10.7 min (Fig. 3A), corresponding to mean particle sizes of 2.3 μm for the commercial SiO_2 MPs, as calculated by the $\log t_R$ and $\log d$ equation (Fig. 3B), which is in good agreement with the nominal value (2.47 μm) provided by the manufacturer. A nearly identical value (2.2 μm) was also obtained by SEM analysis (insert in Fig. 3B). These results clearly indicate that the HF5-based size characterization method has excellent potential and provides reliable results about microparticles to learn about size of the residual fractions of $PM_{2.5}$.

3.3. Quantification of soluble Zn in the SRM incubated in various aqueous media

Determination of the soluble Zn fractions in various media including PW, SNW, and SLF, whose pH values were all preadjusted to pH 5.0, was performed using NIST SRM 1648a. The efficiency of in-line filtration was evaluated by comparing the soluble Zn fraction results obtained by the HF5-UV-ICPOES systems with those obtained by off-line determination in the supernatant after centrifugation at 12000 *g* for 20 min. The obtained results were presented in the supporting information (Table S3), which revealed an excellent agreement between the results obtained with the the two methods. Furthermore, the results indicated that the soluble Zn in the form of ions and complexes or ultrafine particles were efficiently removed during the focusing/relaxation step in HF5. It should be also mentioned that the HF5-UV-ICPOES system is

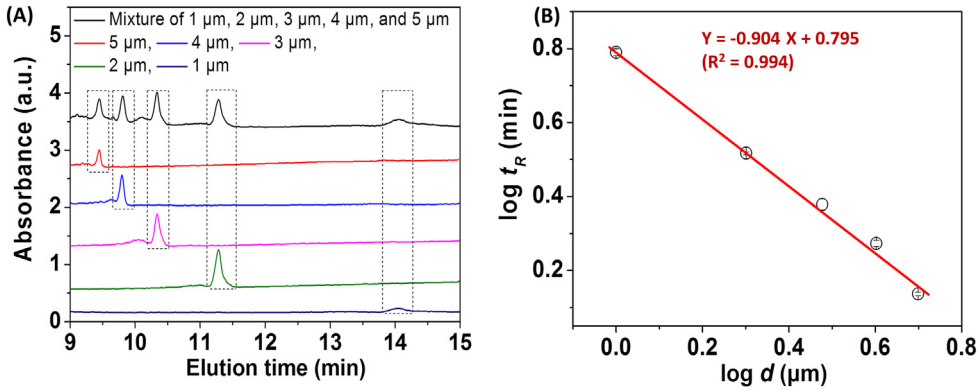

Fig. 2. (A) Fractograms of the PS MPs and their mixture and (B) plot of log t_R (min) vs. log d (μm) of the standards.

superior to the off-line method since it avoids the additional time-consuming centrifugation procedure. Of note, measurement results of the soluble Zn fraction in the supernatant before and after microwave digestion agreed well (data not shown) due to the outstanding capability of ICP for dissociation, atomization and excitation of these Zn species in soluble fractions (Olesik, 1997; Donati et al., 2017).

As expected, there were obvious differences in the dissolution behavior of Zn in the three tested aqueous media with a decreasing order of SLF > PW > SNW (Fig. 4), highlighting the key role of the matrix constituent in dominating the dissolution behavior of Zn in APM. These findings demonstrate much lower stability of Zn in the inhaled APM in the lung than in natural waters, and thus the higher potential health risks. The lower soluble fraction in the NOM solution might be due to the inhibition effects of the NOM coating on Zn ions dissolving from the solid-phase species (Jiang et al., 2015), also suggesting their lower release into the water column and the more probable accumulation in sediments. Because only the total Zn in the NIST SRM 1648a is certified as 4800 mg/kg, the accuracy of the methods was further validated by calculating the mass balance of the soluble and residual fractions of Zn and compared with the certified values. The mean recoveries of Zn ($n = 3$) were between 92.5% and 103%, demonstrating the good accuracy of the HF5-UV-ICPOES method for the soluble Zn determination (Table 1). A *t*-test confirmed that there were no significant differences between the analytical results obtained by the proposed method and the certified values at the 95% confidence level. Additionally, Zn was shown to have mean soluble fractions of 53.5% in SLF, 23.9% in PW, and 14.4% in SNW (Fig. 4), suggesting the easy dissolution and improved mobility of Zn in the SLF. Palacio et al. (2016) reported the high water-soluble fraction of Zn in SRM 1648a subjected to microwave assisted or ultrasonic bath extractions. Similar dissolution profiles of Zn in SRM or APM incubated in various SLF have been found by off-line determination (Dias da Silva et al., 2015; Coufalík et al., 2016). Taken together, the proposed HF5-UV-ICPOES system can serve as a powerful tool for the rapid and accurate evaluation of the dissolution behavior of metals in APM in various aqueous media.

3.4. Determination of soluble Zn and the residual size in $PM_{2.5}$ samples

The advantages of the developed system for accurate size characterization and rapid soluble fraction analysis led us to evaluate the method's practicability in real $PM_{2.5}$ sample analysis. $PM_{2.5}$ samples were obtained from different sites in Beijing and analyzed after 12 h incubation in the three types of the aqueous media. As expected, the soluble Zn fraction and different sized residual particles coexisted in the incubated solutions. The mean soluble and residual Zn contents on the filters, along with their corresponding standard deviations in $PM_{2.5}$ samples, are present in Table 2. Overall, the soluble Zn contents decreased following the order of SLF > PW > SNW for all samples. For the same medium, the soluble Zn concentration in the samples collected from R6 was generally higher than those from the R4 and R2, in line with the higher content of total Zn in the R6 sample (1160 mg/kg) compared with the other two samples (R2, 941 mg/kg, and R4, 970 mg/kg), which were obtained by completely digesting the remaining quarter of the same sample filter followed by ICPOES analysis. In addition to the uncertainty in gravimetric measurements, the uncertainty in the data may mainly come from microwave digestion and ICPOES measurements considering manual operations required for sample handling and analytical protocols as well as any temporary variation in instrumental parameters. The relatively higher Zn content in R6 samples may be correlated with the combustion of coal and biofuels in rural homes and/or autumn-harvest in view of the shorter distance between the sampling site and the closest rural area in addition to the geological differences (Li et al., 2017; Ondo et al., 2013). Correspondingly, the percentage of soluble Zn in R2, R4, and R6 samples ranged from 15.4% to 16.7% in PW, 10.6% to 12.7% in SNW, and 43.1% to 46.9% in SLF, with the trend in good agreement with the findings for NIST SRM 1648a

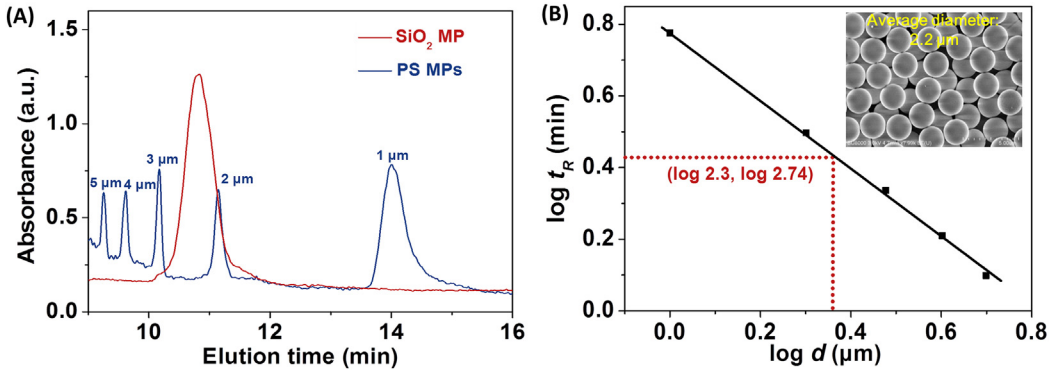

Fig. 3. (A) Fractograms of the PS MPs (1–5 μm) and SiO_2 MPs and (B) comparison of calibration results obtained by HF5-UV-ICPOES and the SEM results.

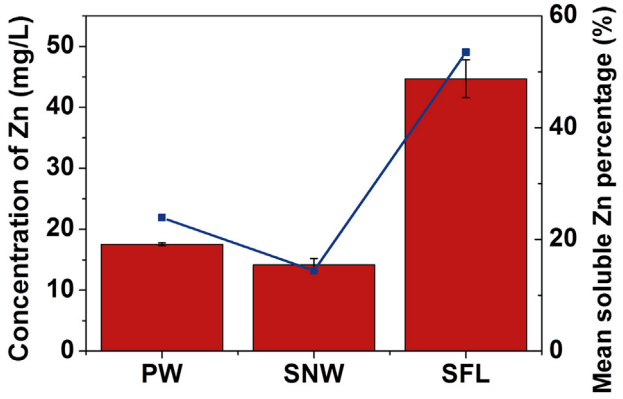

Fig. 4. Evaluation of the dissolution behavior of Zn in NIST SRM 1648a in various aqueous media including pure water (PW), simulated natural water (SNW), and simulated lung fluid (SLF).

above as well as previous studies on Zn solubility from APM (Mukhtar and Limbeck, 2010; Karthikeyan et al., 2006), again indicating the highest solubility in the SLF medium.

Regarding the size of the residual particulate fraction in the three media, no significant changes in elution time (~12.7 min) (Fig. S3), corresponding to 2.4 μm, were observed, indicating that there are still detectable amounts of $PM_{2.5}$ in the media after 12 h incubation; SEM confirmed these results (Fig. S4). In contrast, there are obvious differences in the net peak area count (Fig. S5), which were calculated after subtracting those of the aqueous media alone, eluted in the focusing/relaxation step, due to the release of $PM_{2.5}$ into smaller particles less than the pore size of the HF used (ca. 10 nm), which should be paid more attention due to the much greater environmental and human risk of the ultrafine APM (Allen et al., 2014). Accurate size characterization of the small sized fraction can be performed by collecting eluents during the focusing/relaxation step and off-line characterization by other techniques such as transmission electron microscopy, which is beyond the scope of this study but deserves future investigation. Although the small number of $PM_{2.5}$ samples herein did not reflect the local air quality to more extent, the results show that the method descried herein is a promising tool for the analysis of a larger number of $PM_{2.5}$ samples from a network of sampling sites across various seasons since it is not time consuming and it offers reliable analytical results.

Thorough determination of particulate Zn in the residual $PM_{2.5}$ fractions in addition to the size information could be worthwhile to better understand $PM_{2.5}$ sources and estimate their adverse health effects. Indeed, studies on the association between elemental composition and size information of APM have been reported by several groups (Dallarosa et al., 2008; Rodríguez et al., 2004; Hao et al., 2018). Unfortunately, the proposed method did not give the particulate Zn content in the residual fraction due to the low efficiency of the atomizing system available. Thus, coupling HF5 with the state-of-the-art elemental analyzer equipped with a highly efficient atomizing system would be expected to achieve simultaneous determination of the Zn content in both soluble and residual fraction of $PM_{2.5}$.

Table 1
Dry weight values of soluble and residual Zn after incubation in three various media including pure water (PW), simulated natural water (SNW), and simulated lung fluid (SLF) and the corresponding recovery.

Various media	Soluble fraction[a] (mg/kg)	The residual fraction (mg/kg)	Mean recovery (%)[b]
PW	1060 ± 47.9	3380 ± 204	92.5
SNW	673 ± 40.6	3970 ± 107	96.7
SLF	2660 ± 92.1	2310 ± 118	103

[a] Mean ± standard deviation (SD) (n = 3).
[b] The certified value of NIST is 4800 mg/kg.

4. Conclusions

The HF5-UV-ICPOES system described herein has been successfully applied to quantify soluble Zn and characterize the size of the residual fraction in one run. The experimental results obtained from the quantification of the soluble Zn fraction in NIST SRM 1648a and the size characterization of a commercial SiO_2 MPs demonstrated the accuracy and reliability of the developed method. Due to the characteristic advantages of HF5, efficient in-line filtration and excellent fractionation resolution, the NIST SRM 1648a sample and real $PM_{2.5}$ samples incubated in PW, SNW, and SLF were directly injected, separated, and analyzed by the proposed method, and the calculated soluble Zn fractions was higher for SLF than for PW and SNW. This suggests a much higher dissolution behavior and bioavailability of Zn in physiological environments than in the natural aqueous environment. Moreover, the amount of nanometer-sized APM released from $PM_{2.5}$ followed the order of SLF > PW > SNW, suggesting that $PM_{2.5}$ remained stable in the natural water column and was readily deposited in the sediment. Although only the soluble Zn was quantified using the proposed approach, it is believed that this methodology can be expanded to quantify both the soluble and the residual Zn as well as those of other transition metals by coupling HF5 with other more sensitive detectors such as ICP mass spectroscopy. Collectively, the novel coupling system developed herein provided a powerful tool to quantify the soluble transition metal fractions and obtain the size information of the residual fraction in short analysis time, demonstrating its great potential applications in monitoring air pollution. Additionally, this work proposed a promising approach for an in-depth understanding of the health risks associated with $PM_{2.5}$ samples given the close correlation between its transition metal contents and morbidity. Preliminary investigation has shown a discrepancy in soluble Zn content among different functional zones. Therefore, future studies will be needed to evaluate the dissolution behaviors of other transition metals in a larger number of $PM_{2.5}$ collected from greater sampling network to evaluate air quality and further conduct source apportionment studies; this is already being performed in an ongoing study.

CRediT authorship contribution statement

Zhiqiang Tan: Conceptualization, Methodology, Writing - original draft.**Qingsheng Bai:**Investigation, Data curation.**Yongguang Yin:**Validation.**Yang Zhang:**Resources.**Qiang Chen:**Visualization.**Myeong Hee Moon:**Formal analysis.**Jingfu Liu:**Writing - review & editing.

Declaration of competing interest

The authors declare that they have no known competing financial interests or personal relationships that could have appeared to influence the work reported in this paper.

Acknowledgments

This work was supported by the National Key R&D Program of China (no. 2018YFC1602305) and the National Natural Science Foundation of China (nos. 21577150 and 21827815). Z.T. also acknowledges the support from the Youth Innovation Promotion Association CAS (2017065). The authors sincerely thank the anonymous reviewers for valuable comments and suggestions on this paper.

Appendix A. Supplementary data

Supplementary data to this article can be found online at https://doi.org/10.1016/j.scitotenv.2020.138309.

Table 2
Dry weight values of soluble and residual Zn in $PM_{2.5}$ samples after incubation in three various media including pure water (PW), simulated natural water (SNW), and simulated lung fluid (SLF). (mg/kg) (value = mean ± SD, $n = 3$).

Various media	R2		R4		R6	
	Soluble	Residual	Soluble	Residual	Soluble	Residual
PW	143 ± 11.5	782 ± 13.8	168 ± 10.7	835 ± 18.6	164 ± 10.9	880 ± 15.6
SNW	101 ± 5.0	856 ± 27.2	113 ± 7.9	871 ± 23.1	136 ± 6.0	941 ± 15.9
SLF	430 ± 32.5	485 ± 30.7	453 ± 23.9	528 ± 33.7	483 ± 39.9	636 ± 39.9

References

Akimoto, H., 2003. Global air quality and pollution. Science 302, 1716–1719.

Allen, J.L., Liu, X.F., Pelkowski, S., Palmer, B., Conrad, K., Oberdorster, G., Weston, D., Mayer-Proschel, M., Cory-Slechta, D.A., 2014. Early postnatal exposure to ultrafine particulate matter air pollution: persistent ventriculomegaly, neurochemical disruption, and glial activation preferentially in male mice. Environ. Health Persp. 122, 939–945.

Amini, H., Nhung, N.T.T., Schindler, C., Yunesian, M., Hosseini, V., Shamsipour, M., Hassanvand, M.S., Mohammadi, Y., Farzadfar, F., Vicedo-Cabrera, A.M., Schwartz, J., Henderson, S.B., Kunzli, N., 2019. Short-term associations between daily mortality and ambient particulate matter, nitrogen dioxide, and the air quality index in a Middle Eastern megacity. Environ. Pollut. 254, 113121 UNSP.

Bell, M.L., Dominici, F., Ebisu, K., Zeger, S.L., Samet, J.M., 2007. Spatial and temporal variation in $PM_{2.5}$ chemical composition in the United States for health effects studies. Environ. Health Persp. 115, 989–995.

Bressi, M., Sciare, J., Ghersi, V., Bonnaire, N., Nicolas, J.B., Petit, J.E., Moukhtar, S., Rosso, A., Mihalopoulos, N., Feron, A., 2013. A one-year comprehensive chemical characterisation of fine aerosol ($PM_{2.5}$) at urban, suburban and rural background sites in the region of Paris (France). Atmos. Chem. Phys. 13, 7825–7844.

van Bruijnsvoort, M., Kok, W.T., Tijssen, R., 2001. Hollow-fiber flow field-flow fractionation of synthetic polymers in organic solvents. Anal. Chem. 73, 4736–4742.

Calderon-Garciduenas, L., Solt, A.C., Henriquez-Roldan, C., Torres-Jardon, R., Nuse, B., Herritt, L., Villarreal-Calderon, R., Osnaya, N., Stone, I., Garcia, R., Brooks, D.M., Gonzalez-Maciel, A., Reynoso-Robles, R., Delgado-Chavez, R., Reed, W., 2008. Long-term air pollution exposure is associated with neuroinflammation, an altered innate immune response, disruption of the blood-brain barrier, ultrafine particulate deposition, and accumulation of amyloid β-42 and α-synuclein in children and young adults. Toxicol. Pathol. 36, 289–310.

Carlshaf, A., Jönsson, J.Å., 1991. Effects of ionic-strength of eluent on retention behavior and on the peak broadening process in hollow fiber flow field-flow fractionation. J. Microcolumn Sep. 3, 411–416.

Castro-Jimenez, J., Barhoumi, B., Paluselli, A., Tedetti, M., Jimenez, B., Munoz-Arnanz, J., Wortham, H., Driss, M.R., Sempere, R., 2017. Occurrence, loading, and exposure of atmospheric particle-bound POPs at the African and European edges of the western mediterranean sea. Environ. Sci. Technol. 51, 13180–13189.

Chan, K.L., Jiang, S.Y.N., Ning, Z., 2016. Speciation of water soluble iron in size segregated airborne particulate matter using LED based liquid waveguide with a novel dispersive absorption spectroscopic measurement technique. Anal. Chim. Acta 914, 100–109.

Colombo, C., Monhemius, A.J., Plant, J.A., 2008. Platinum, palladium and rhodium release from vehicle exhaust catalysts and road dust exposed to simulated lung fluids. Ecotox. Environ. Safe. 71, 722–730.

Coufalík, P., Mikuška, P., Matoušek, T., Večeřa, Z., 2016. Determination of the bioaccessible fraction of metals in urban aerosol using simulated lung fluids. Atmos. Environ. 140, 469–475.

Dallarosa, J., Teixeira, E.C., Meira, L., Wiegand, F., 2008. Study of the chemical elements and polycyclic aromatic hydrocarbons in atmospheric particles of PM_{10} and $PM_{2.5}$ in the urban and rural areas of South Brazil. Atmos. Res. 89, 76–92.

Dias da Silva, L.I., Yokoyama, L., Maia, L.B., Monteiro, M.I.C., Pontes, F.V.M., Cameiro, M.C., Neto, A.A., 2015. Evaluation of bioaccessible heavy metal fractions in PM_{10} from the metropolitan region of Rio de Janeiro city, Brazil, using a simulated lung fluid. Microchem. J. 118, 266–271.

Donati, G.L., Amais, R.S., Williams, C.B., 2017. Recent advances in inductively coupled plasma optical emission spectrometry. J. Anal. Atom. Spectrom. 32, 1283–1296.

Dubascoux, S., Von Der Kammer, F., Le Hecho, I., Gautier, M.P., Lespes, G., 2008. Optimisation of asymmetrical flow field flow fractionation for environmental nanoparticles separation. J. Chromatogr. A 1206, 160–165.

Fedotov, P.S., Ermolin, M.S., Karandashev, V.K., Ladonin, D.V., 2014. Characterization of size, morphology and elemental composition of nano-, submicron, and micron particles of street dust separated using field-flow fractionation in a rotating coiled column. Talanta 130, 1–7.

Fedotov, P.S., Ermolin, M.S., Katasonova, O.N., 2015. Field-flow fractionation of nano- and microparticles in rotating coiled columns. J. Chromatogr. A 1381, 202–209.

Fuzzi, S., Baltensperger, U., Carslaw, K., Decesari, S., van Der Gon, H.D., Facchini, M.C., Fowler, D., Koren, I., Langford, B., Lohmann, U., Nemitz, E., Pandis, S., Riipinen, I., Rudich, Y., Schaap, M., Slowik, J.G., Spracklen, D.V., Vignati, E., Wild, M., Williams, M., Gilardoni, S., 2015. Particulate matter, air quality and climate: lessons learned and future needs. Atmos. Chem. Phys. 15, 8217–8299.

Gao, P., Guo, H.Y., Zhang, Z.H., Ou, C.Y., Hang, J., Fan, Q., He, C., Wu, B., Feng, Y.J., Xing, B.S., 2018. Bioaccessibility and exposure assessment of trace metals from urban airborne particulate matter (PM_{10} and $PM_{2.5}$) in simulated digestive fluid. Environ. Pollut. 242, 1669–1677.

Giddings, J.C., 1993. Field-flow fractionation - analysis of macromolecular, colloidal, and particulate materials. Science 260, 1456–1465.

Gu, X.Y., Chu, X., Zeng, X.L., Bao, H.R., Liu, X.J., 2017. Effects of $PM_{2.5}$ exposure on the Notch signaling pathway and immune imbalance in chronic obstructive pulmonary disease. Environ. Pollut. 226, 163–173.

Gupta, P., Christopher, S.A., Wang, J., Gehrig, R., Lee, Y., Kumar, N., 2006. Satellite remote sensing of particulate matter and air quality assessment over global cities. Atmos. Environ. 40, 5880–5892.

Hao, Y.F., Meng, X.P., Yu, X.P., Lei, M.L., Li, W.J., Shi, F.T., Yang, W.W., Zhang, S.J., Xie, S.D., 2018. Characteristics of trace elements in $PM_{2.5}$ and PM_{10} of Chifeng, northeast China: insights into spatiotemporal variations and sources. Atmos. Res. 213, 550–561.

Hu, X., Zhang, Y., Ding, Z.H., Wang, T.J., Lian, H.Z., Sun, Y.Y., Wu, J.C., 2012. Bioaccessibility and health risk of arsenic and heavy metals (Cd, Co, Cr, Cu, Ni, Pb, Zn and Mn) in TSP and $PM_{2.5}$ in Nanjing, China. Atmos. Environ. 57, 146–152.

Huang, W., Zhang, Y.X., Zhang, Y., Zeng, L.M., Dong, H.B., Huo, P., Fang, D.Q., Schauer, J.J., 2016. Development of an automated sampling-analysis system for simultaneous measurement of reactive oxygen species (ROS) in gas and particle phases: GAC-ROS. Atmos. Environ. 134, 18–26.

Jiang, C.J., Aiken, G.R., Hsu-Kim, H., 2015. Effects of natural organic matter properties on the dissolution kinetics of zinc oxide nanoparticles. Environ. Sci. Technol. 49, 11476–11484.

Karthikeyan, S., Joshi, U.M., Balasubramanian, R., 2006. Microwave assisted sample preparation for determining water-soluble fraction of trace elements in urban airborne particulate matter: evaluation of bioavailability. Anal. Chim. Acta 576, 23–30.

Kim, H.J., Oh, S., Moon, M.H., 2006. Hollow-fiber flow/hyperlayer field-flow fractionation for the size characterization of airborne particle fractions obtained by SPLITT fractionation. J. Sep. Sci. 29, 423–428.

Kim, S.T., Rah, K., Lee, S., 2012. Effect of surfactant on retention behaviors of polystyrene latex particles in sedimentation field-flow fractionation: effective boundary slip model approach. Langmuir 28, 10672–10681.

Kim, K.H., Kabir, E., Kabir, S., 2015. A review on the human health impact of airborne particulate matter. Environ. Int. 74, 136–143.

Lee, W.J., Min, B.R., Moon, M.H., 1999. Improvement in particle separation by hollow fiber flow field-flow fractionation and the potential use in obtaining particle site distribution. Anal. Chem. 71, 3446–3452.

Li, R., Li, J.L., Cui, L.L., Wu, Y., Fu, H.B., Chen, J.M., Chen, M.D., 2017. Atmospheric emissions of Cu and Zn from coal combustion in China: spatio-temporal distribution, human health effects, and short-term prediction. Environ. Pollut. 229, 724–734.

Loxham, M., Cooper, M.J., Gerlofs-Nijland, M.E., Cassee, F.R., Davies, D.E., Palmer, M.R., Teagle, D.A.H., 2013. Physicochemical characterization of airborne particulate matter at a mainline underground railway station. Environ. Sci. Technol. 47, 3614–3622.

Maret, W., Sandstead, H.H., 2006. Zinc requirements and the risks and benefits of zinc supplementation. J. Trace Elem. Med. Bio. 20, 3–18.

Min, B.R., Kim, S.J., Ahn, K.H., Moon, M.H., 2002. Hyperlayer separation in hollow fiber flow field-flow fractionation: effect of membrane materials on resolution and selectivity. J. Chromatogr. A 950, 175–182.

Mukhtar, A., Limbeck, A., 2010. On-line determination of water-soluble zinc in airborne particulate matter using a dynamic extraction procedure coupled to flame atomic absorption spectrometry. J. Anal. Atom. Spectrom. 25, 1056–1062.

Olesik, J.W., 1997. Investigating the fate of individual sample droplets in inductively coupled plasmas. Appl. Spectrosc. 51, 158A–175A.

Ondo, J.A., Biyogo, R.M., Eba, F., Prudent, P., Fotio, D., Ollui-Mboulou, M., Omva-Zue, J., 2013. Accumulation of soil-borne aluminium, iron, manganese and zinc in plants cultivated in the region of Moanda (Gabon) and nutritional characteristics of the edible parts harvested. J. Sci. Food Agr. 93, 2549–2555.

Palacio, I.C., Oliveira, I.F., Franklin, R.L., Barros, S.B.M., Roubicek, D.A., 2016. Evaluating the mutagenicity of the water-soluble fraction of air particulate matter: a comparison of two extraction strategies. Chemosphere 158, 124–130.

Porea, T.J., Belmont, J.W., Mahoney Jr., D.H., 2000. Zinc-induced anemia and neutropenia in an adolescent. J. Pediatr. 136, 688–690.

Pun, V.C., Kazemiparkouhi, F., Manjourides, J., Suh, H.H., 2017. Long-term $PM_{2.5}$ exposure and respiratory, cancer, and cardiovascular mortality in older US adults. Am. J. Epidemiol. 186, 961–969.

Reschiglian, P., Roda, B., Zattoni, A., Min, B.R., Moon, M.H., 2002. High performance, disposable hollow fiber flow field-flow fractionation for bacteria and cells. First application to deactivated *Vibrio cholera*. J. Sep. Sci. 25, 490–498.

Reschiglian, P., Zattoni, A., Roda, B., Cinque, L., Melucci, D., Min, B.R., Moon, M.H., 2003. Hyperlayer hollow-fiber flow field-flow fractionation of cells. J. Chromatogr. A 985, 519–529.

Rice, T.M., Clarke, R.W., Godleski, J.J., Al-Mutairi, E., Jiang, N.F., Hauser, R., Paulauskis, J.D., 2001. Differential ability of transition metals to induce pulmonary inflammation. Toxicol. Appl. Pharm. 177, 46–53.

Rodríguez, S., Querol, X., Alastuey, A., Viana, M.M., Alarcón, M., Mantilla, E., Ruiz, C.R., 2004. Comparative PM10-PM2.5 source contribution study at rural, urban and industrial sites during PM episodes in Eastern Spain. Sci. Total Environ. 328, 95–113.

Rychlik, M., Mlyniec, K., 2020. Zinc-mediated neurotransmission in Alzheimer's disease: a potential role of the GPR39 in dementia. Curr. Neuropharmacol. 18, 2–13.

Shen, M.H., Yin, Y.G., Booth, A., Liu, J.F., 2015. Effects of molecular weight-dependent physicochemical heterogeneity of natural organic matter on the aggregation of fullerene nanoparticles in mono- and di-valent electrolyte solutions. Water Res. 71, 11–20.

Song, W.H., Zhang, J.Y., Guo, J., Zhang, J.H., Ding, F., Li, L.Y., Sun, Z.T., 2010. Role of the dissolved zinc ion and reactive oxygen species in cytotoxicity of ZnO nanoparticles. Toxicol. Lett. 199, 389–397.

Song, C.B., He, J.J., Wu, L., Jin, T.S., Chen, X., Li, R.P., Ren, P.P., Zhang, L., Mao, H.J., 2017. Health burden attributable to ambient $PM_{2.5}$ in China. Environ. Pollut. 223, 575–586.

Stevenson, S.G., Preston, K.R., 1997. Effects of surfactants on wheat protein fractionation by flow field-flow fractionation. J. Liq. Chromatogr. R. T. 20, 2835–2842.

Stone, V., Johnston, H., Clift, M.J.D., 2007. Air pollution, ultrafine and nanoparticle toxicology: cellular and molecular interactions. IEEE T. Nanobiosci. 6, 331–340.

Suarez-Varela, M.M., Llopis-González, A., González Albert, V., López-Izquierdo, R., González-Manzano, I., Cháves, J., Biosca, V.H., Martin-Escudero, J.C., 2015. Zinc and smoking habits in the setting of hypertension in a Spanish populations. Hypertens. Res. 38, 149–154.

Tan, Z.Q., Liu, J.F., Guo, X.R., Yin, Y.G., Byeon, S.K., Moon, M.H., Jiang, G.B., 2015. Toward full spectrum speciation of silver nanoparticles and ionic silver by on-line coupling of hollow fiber flow field-flow fractionation and minicolumn concentration with multiple detectors. Anal. Chem. 87, 8441–8447.

Tan, Z.Q., Yin, Y.G., Guo, X.R., Amde, M., Moon, M.H., Liu, J.F., Jiang, G.B., 2017. Tracking the transformation of nanoparticulate and ionic silver at environmentally relevant concentration levels by hollow fiber flow field-flow fractionation coupled to ICPMS. Environ. Sci. Technol. 51, 12369–12376.

World Health Organization (WHO), 2006. Air Quality Guidelines for particulate matter, ozone, nitrogen dioxide and sulfur dioxide. Global Update 2005. Summary of Risk Assessment.

Yang, X.Z., Liu, X., Zhang, A.Q., Lu, D.W., Li, G., Zhang, Q.H., Liu, Q., Jiang, G.B., 2019. Distinguishing the sources of silica nanoparticles by dual isotopic fingerprinting and machine learning. Nat. Commun. 10, 1620.

Zattoni, A., Casolari, S., Rambaldi, D.C., Reschiglian, P., 2007. Hollow-fiber flow field-flow fractionation. Curr. Anal. Chem. 3, 310–323.

Zattoni, A., Rambaldi, D.C., Roda, B., Parisi, D., Roda, A., Moon, M.H., Reschiglian, P., 2008. Hollow-fiber flow field-flow fractionation of whole blood serum. J. Chromatogr. A 1183, 135–142.

Zereini, F., Wiseman, C.L.S., Puttmann, W., 2012. In vitro investigations of platinum, palladium, and rhodium mobility in urban airborne particulate matter (PM_{10}, $PM_{2.5}$, and PM_1) using simulated lung fluids. Environ. Sci. Technol. 46, 10326–10333.

Zhang, Q., Zheng, Y.X., Tong, D., Shao, M., Wang, S.X., Zhang, Y.H., Xu, X.D., Wang, J.N., He, H., Liu, W.Q., Ding, Y.H., Lei, Y., Li, J.H., Wang, Z.F., Zhang, X.Y., Wang, Y.S., Cheng, J., Liu, Y., Shi, Q.R., Yan, L., Geng, G.N., Hong, C.P., Li, M., Liu, F., Zheng, B., Cao, J.J., Ding, A.J., Gao, J., Fu, Q.Y., Huo, J.T., Liu, B.X., Liu, Z.R., Yang, F.M., He, K.B., Hao, J.M., 2019. Drivers of improved $PM_{2.5}$ air quality in China from 2013 to 2017. Proc. Natl. Acad. Sci. 116, 24463–24469.